Research Article Vol. 58, No. 12 / 20 April 2019 / Applied Optics 3193

applied optics

# Fast method to detect and calculate displacement errors in a Littrow grating-based interferometer

Qiang Lv,[1,2] Zhaowu Liu,[1] Wei Wang,[1] Shan Jiang,[1] Bayanheshig,[1] and Wenhao Li[2,*]

[1]Changchun Institute of Optics, Fine Mechanics and Physics, Chinese Academy of Sciences, Changchun, Jilin 130033, China
[2]University of Chinese Academy of Sciences, Beijing 100049, China
*Corresponding author: liwh@ciomp.ac.cn

Received 17 January 2019; revised 11 March 2019; accepted 25 March 2019; posted 26 March 2019 (Doc. ID 358024); published 17 April 2019

**Grating-based interferometers play important roles in precision displacement measurements. Gratings are the core components of grating-based interferometers, and grating surface errors and line errors seriously affect measurement accuracy, especially in systems with Littrow configurations. A fast, accurate method to calculate displacement errors caused by grating surface errors and line errors in a grating-based interferometer with a Littrow configuration is proposed. Displacement errors are calculated using the diffracted wavefronts at the ±1st orders of the grating. Experimental comparison of the displacements of a grating-based interferometer and a laser interferometer verifies the correctness of the proposed method. The differences between the calculated and measured displacement error results are within 40 nm. The method is accurate, fast, and low cost and is highly significant for system error compensation and improvement of the measurement accuracy of grating-based interferometers.** 

https://doi.org/10.1364/AO.58.003193

## 1. INTRODUCTION

Precision displacement measurement technology plays highly important roles in numerous fields [1–5]. The grating-based interferometer (GI) [6–10], which uses the grating period as its measurement datum, is less strongly affected by the environment than the laser interferometer (LI), which uses the wavelength as its datum [11,12]. The GI, thus, has very wide application prospects.

In the GI, there are two main ways in which the laser beam can be incident on the grating: vertical incidence and oblique incidence. Based on the auto-collimation principle, the method in which the beam is incident on the grating at the Littrow angle is widely used in oblique incidence applications. There are several examples of GIs that have been designed using Littrow configurations [13–17]. When compared with vertical incidence, this method offers many advantages. It can improve the laser energy utilization; gratings with higher line densities can be used for the same wavelength, which gives these GIs higher resolution; and the distance between the reading head and the grating is not strictly controlled, which makes installation simpler. However, this method also has some shortcomings. When the two beam spots coincide on the grating, zero-order diffraction light will return to the receiver along with the measurement beam, which has a serious effect on measurement signal collection. In a heterodyne GI with a Littrow configuration, imperfect optical elements and the grating polarization characteristics can also cause zero-order diffraction light to enter the receiver. The system then cannot distinguish the measurement signals and thus cannot measure the displacement. Therefore, it is necessary to adjust the distance between the grating and the reading head to ensure that the two beam spots on the grating are separated by a specific distance; this is the simplest and most effective way to prevent zero-order diffraction light from entering the receiver. However, because of the limitations of grating manufacturing technology, gratings are not perfect, and surface errors and line errors are present in gratings. The grating surface error is the out-of-flatness error of the grating and is mainly determined by the grating substrate. Grating line errors are caused by pitch deviations in the grating. These pitch deviations are mainly caused during grating fabrication. The out-of-flatness errors and pitch deviations of the grating will then make the diffraction wavefront imperfect. Because of the different positions of the two spots on the grating, any additional optical path difference caused by an imperfect grating becomes a displacement measurement error. With the ongoing improvements in measurement range, precision, and resolution of the GI, this effect cannot be ignored.

The displacement error that is caused by a grating surface error and/or line error can be calibrated using a LI in a vacuum [18]. By comparing measured data from two systems, the grating accuracy can be calibrated precisely. However, the cost

of this method is high, and the system required is complex. A scanning probe microscope [19,20] can be used to image very small areas of the error region, but it is highly impractical to use this method to detect the surface and line conditions over the entire grating because of the microscope's slow scanning speed and small observation range. Grating errors can be reflected directly onto the diffraction wavefront, such that the diffraction wavefront error is mainly composed of the grating surface error and line errors [21–23]. Gao *et al.* proposed a method to evaluate the surface errors and line errors of gratings based on diffraction wavefronts obtained using a Fizeau interferometer [24]. They also verified their method experimentally using a three-dimensional (3D) GI. However, the laser beam was vertically incident on the grating in the 3D GI, and the surface error, thus, only affects the displacement perpendicular to the grating plane, while the line error only affects the displacement parallel to the grating plane. This does not apply to a GI in the Littrow configuration. Further in-depth analysis of the relationship between the grating error and the displacement error is thus required.

In this paper, we propose a fast and accurate method to calculate the displacement error caused by the grating surface error and line errors in a GI using the Littrow configuration and propose a theoretical model to perform error analysis. The correctness of the method is verified experimentally. This method is of major significance for compensation of system errors and enhancement of the measurement accuracy of GIs.

## 2. PRINCIPLE

As shown in Fig. 1, the intensity signal received by the GI is given by

$$I \propto \cos(\phi_v + \phi_{ge} + \phi_e), \tag{1}$$

where $I$ is the interference field intensity, $\phi_v$ is the phase change caused by the grating motion based on the Doppler principle, and $\phi_{ge}$ is the phase change caused by the grating errors. $\phi_e$ is the phase change caused by other aspects, such as linear stage errors and changes in the surrounding environment.

The relationship between the phase change and the displacement caused by the grating motion is

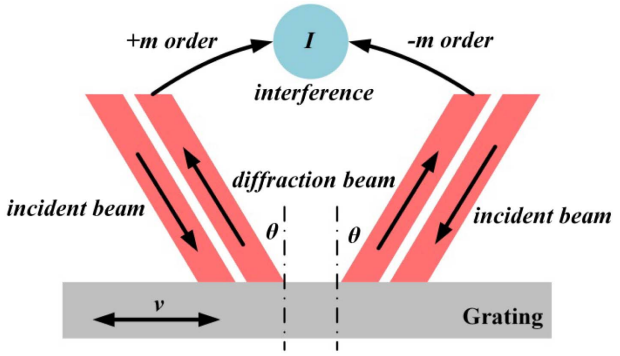


**Fig. 1.** Schematic diagram of GI in Littrow configuration. Incoming beams are incident on the grating at the Littrow angle, and the diffracted beams return along the original path and interfere. When the grating moves at a speed $v$, the interference field $I$ will change.

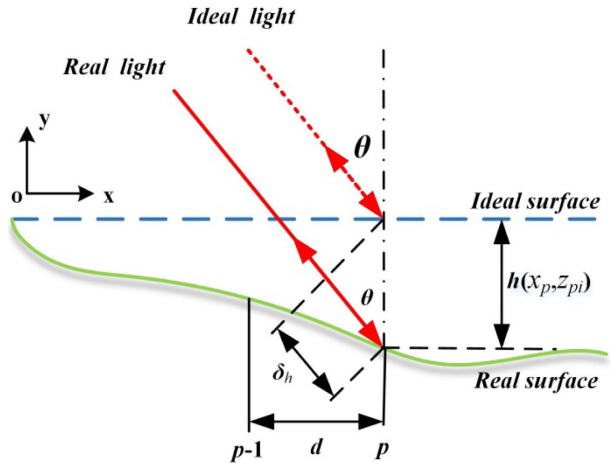


**Fig. 2.** Optical path changes induced by surface error.

$$\phi_v + \phi_{ge} + \phi_e = \frac{4\pi m}{d}(l + l_{ge} + l_e), \tag{2}$$

where $m = 0, 1, 2, 3\ldots, l$ is the grating displacement, $l_{ge}$ is the displacement error caused by the grating surface error and line errors, $l_e$ is the displacement error caused by the other conditions, and $d$ is the grating period.

Figures 2 and 3 show schematic diagrams of the optical path changes induced by a surface error and a line error, respectively. The beam is incident on the grating at the Littrow angle in each case. The grating groove direction is parallel to the $Z$ axis. As shown in Fig. 2, when there is a depth difference $h(x_p, z_{pi})$ between the real surface and the ideal surface at any point $i$ on the $p$th line of the grating, the optical path difference $\delta_h$ between the ideal light beam and the real light beam at this point is

$$\delta_h = 2h(x_p, z_{pi}) \cos\theta_m, \tag{3}$$

where $\theta_m$ is the angle of incidence.

As shown in Fig. 3, when there is a line error but no surface error in the grating, the distance between the actual position and the ideal position at any point $i$ on the $p$th line of the grating is $w(x_p, z_{pi})$. The optical path difference $\delta_l$ between the ideal light beam and the real light beam at this point is

$$\delta_l = 2w(x_p, z_{pi}) \sin\theta_m. \tag{4}$$

By combining the above with the grating equation $2d \sin\theta_m = m\lambda$, Eq. (4) can be changed to read

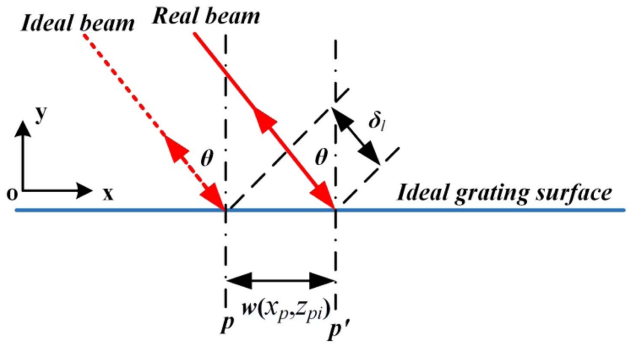


**Fig. 3.** Optical path changes induced by line error.

$$\delta_l = w(x_p, z_{pi})\frac{m\lambda}{d}, \tag{5}$$

where $m$ is the diffraction order, with $m = 0, 1, 2, 3\ldots$, and $\lambda$ is the wavelength.

Using the matrices $\mathbf{H}$ and $\mathbf{W}$ to represent the grating surface error and the line error, respectively, we can obtain the following mathematical expression for the diffraction wavefronts of the $\pm m$th orders:

$$\mathbf{\Delta}(\pm m) = 2\mathbf{H}\cos\theta_m \pm \mathbf{W}\frac{m\lambda}{d}, \tag{6}$$

where $\mathbf{\Delta}(\pm m)$ denotes the diffraction wavefronts of the $\pm m$th orders.

Because the Littrow structure is used, the positions of the two beam spots on the grating in the GI are different, and the two diffraction wavefronts are thus produced at different grating positions. The phase error $\phi_{ge}$ can be expressed as

$$\phi_{ge} = \frac{2\pi}{\lambda'}[\mathbf{\Delta_1}(+n) - \mathbf{\Delta_2}(-n)], \tag{7}$$

where $\lambda'$ is the wavelength used in the GI, $\pm n$ are the diffraction orders, where $n = 0, 1, 2, 3\ldots$, and $\mathbf{\Delta_1}(+n)$ and $\mathbf{\Delta_2}(-n)$ are the diffractive wavefronts of the two beams, which can be calculated using

$$\begin{cases} \mathbf{\Delta_1}(+n) = 2\mathbf{H_1}\cos\theta_n + \mathbf{W_1}n\lambda'/d \\ \mathbf{\Delta_2}(-n) = 2\mathbf{H_2}\cos\theta_n - \mathbf{W_2}n\lambda'/d \end{cases}, \tag{8}$$

where $\theta_n$ is the Littrow angle, and $\mathbf{H_1}$ and $\mathbf{W_1}$ are the surface error and the line error of the grating that are covered by the first spot. $\mathbf{H_2}$ and $\mathbf{W_2}$ are the surface error and the line error of the grating that are covered by the second spot. $\mathbf{H_1}$, $\mathbf{H_2}$, $\mathbf{W_1}$, and $\mathbf{W_2}$ can all be extracted from the overall surface error and line error that can be obtained from Eq. (6).

It can be determined from Eqs. (2) and (7) that when the grating moves, the relationship between the diffraction wavefront and the displacement error is

$$\mathbf{l_{ge}} = [\mathbf{\Delta_1}(+n) - \mathbf{\Delta_2}(-n)]\frac{d}{2n\lambda'}, \tag{9}$$

and by combining Eqs. (8) and (9) with the grating equation $2d\sin\theta_n = n\lambda'$, we then obtain

$$\mathbf{l_{ge}} = \frac{1}{2\tan\theta_n}(\mathbf{H_1} - \mathbf{H_2}) + \frac{1}{2}(\mathbf{W}_1 + \mathbf{W}_2). \tag{10}$$

Equation (10) shows that the surface error and the line error of the grating both affect the displacement. When the two spots overlap completely, i.e., when $\mathbf{H_1} = \mathbf{H_2} = \mathbf{H}$ and $\mathbf{W_1} = \mathbf{W_2} = \mathbf{W}$, Eq. (10) will then become $\mathbf{l_{ge}} = \mathbf{W}$. The displacement error is thus caused solely by the line error. This is consistent with a GI in which the beam is perpendicularly incident on the grating.

Therefore, when calculating the displacement error caused by the grating surface error and the line error in a GI in the Littrow configuration, we must first obtain the diffraction wavefronts of the symmetric orders using an interferometer. We must then extract the wavefronts that are covered by the two spots from the wavefronts that were obtained previously. If the wavelength of the interferometer differs from that of the GI, we should calculate the surface error and the line error of the grating using Eq. (6). We can then calculate the displacement error using Eq. (10). When the wavelength of the interferometer is the same as that of the GI, we do not need to calculate the surface error or the line error. We can calculate the displacement error directly using Eq. (9) and the diffracted wavefronts. Use of the method described above means that we do not require expensive experimental facilities or a complex series of steps, which greatly reduces the cost and difficulty of the operation and is helpful for error compensation.

## 3. EXPERIMENTAL

To verify that the proposed method is both correct and accurate, we designed an experiment to compare the measured results with the calculated results in terms of the displacement error. The experiment consisted of two main parts: (1) measurement of the displacement error and (2) calculation of the displacement error. First, we obtained the displacement difference between the heterodyne GI with the Littrow configuration and the dual-frequency LI via a comparison experiment. Then, we calculated the displacement error using the diffraction wavefronts of the grating. Finally, we compared the results that were obtained using these two methods.

In the first part of the experiment, we designed an experiment to enable comparison of the displacement measurements of the GI and the LI. The experimental setup is shown in Fig. 4. The LI is located within the blue dotted line and includes a plane mirror interferometer (10706B, Agilent), a mirror ($M_3$), and a receiver ($R_1$). The GI with the Littrow configuration is located within the white dashed line. This GI includes an integrated module that contains a polarizing beam splitter and two quarter-wave plates (PBS&QW), two mirrors ($M_4$ and $M_5$), a reflection grating (a reproduction grating made in our own laboratory) with dimensions of 50 mm × 25 mm × 6 mm and a line density of 1800 lines/mm, and a receiver ($R_2$). The receivers $R_1$ and $R_2$ are both Agilent 10780F remote receivers. The receivers' lenses and polarizers are contained within small assemblies that are connected to their electronic housings via fiber optic cables. These fiber optic cables allow the receiver modules to be mounted away from the measurement area, thus removing a potential source of heat. The receivers convert the Doppler-shifted laser light into electrical signals that can be

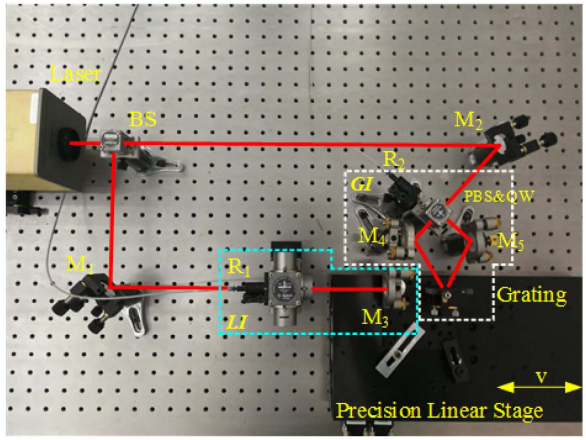


**Fig. 4.** Experimental setup for displacement measurements.

processed by the rest of the system. $M_3$ and the grating are fixed on a precision linear stage (XML210-s, Newport). The surface of $M_3$ lies perpendicular to the grating surface. To reduce the Abbe error, the positions of the beam spots on $M_3$ and on the grating lie in a straight line along the direction of motion. A He–Ne laser ($\lambda = 632.8$ nm, beam spot diameter of 6 mm) is used as the light source. When the precision linear stage moves, both the LI and the GI can measure the displacement. The in-house-made board can process the displacement signals of the LI and GI simultaneously. We use LabVIEW software to extract the displacement data from the two systems simultaneously and to calculate the measurement differences between the two systems. In this experiment, we believe that the measurements made by the LI are accurate, so any difference between the displacement measurement results of the two systems can be regarded as the GI displacement error. To ensure measurement accuracy, the experimental equipment is set up on an air floatation platform and is sealed to minimize the effects of the surroundings.

The positions of the reading head and the grating are adjusted such that the centers of the two spots on the grating are spaced 8 mm apart. The positions of the two spots that are tangential to the edge of the grating are then set as the start and end points of the motion. The range of the GI is thus 36 mm. We set the speed of the precision linear stage at 1 mm/s and its acceleration at 1 mm/s$^2$. To verify the correctness of the theoretical model more forcefully, we adjust the distance between the reading head and the grating such that the two incident beams are in two different states, called separated incidence and crossed incidence, as illustrated in Figs. 5 and 6, respectively. The sequences of the two spots are different, and the effects of the surface error and the line error on the displacement measurements should also be different, so we can obtain two different sets of displacement error results.

Figures 7 and 8 show the displacements that were measured using the LI and the GI. The figures show that both the GI and the LI measured displacements of 36 mm and that the displacement measurement curves of the two systems were closely coincident. However, there are nanoscale differences between the displacements that were measured by these two systems. These differences may be caused by many factors, such as grating surface errors, line errors, accuracy of the linear stage, environmental variations, and electronic noise.

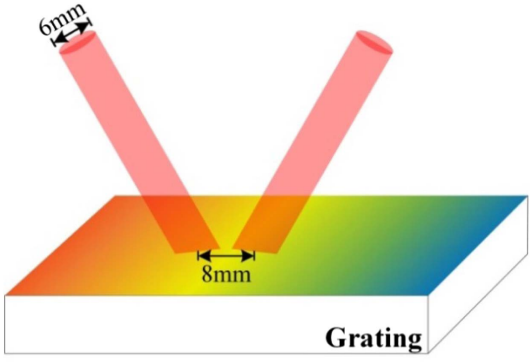


**Fig. 5.** Incident states of the two beams: separated incidence.

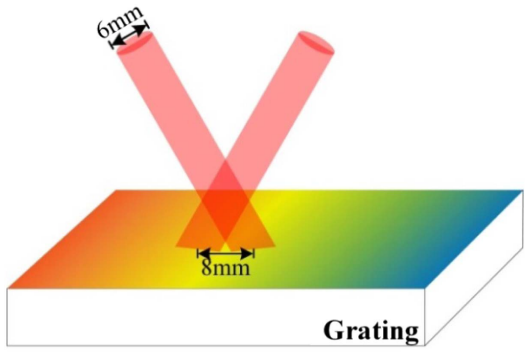


**Fig. 6.** Incident states of the two beams: crossed incidence.

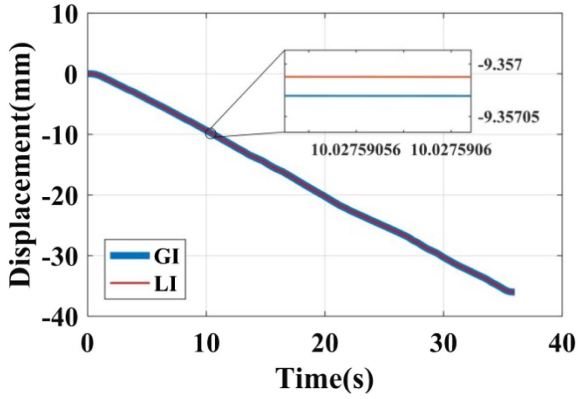


**Fig. 7.** Displacements measured using the LI and the GI. The red line represents the displacement measured by the GI with two incident beams in the separated state. The blue line represents the displacement measured by the LI.

In the second part of the experiment, we use a Zygo interferometer at an operating wavelength of 632.8 nm with error repeatability of $\lambda/10,000$ ($2\sigma$) to obtain the diffraction wavefronts of the $\pm 1$ st orders, with results as shown in Fig. 9.

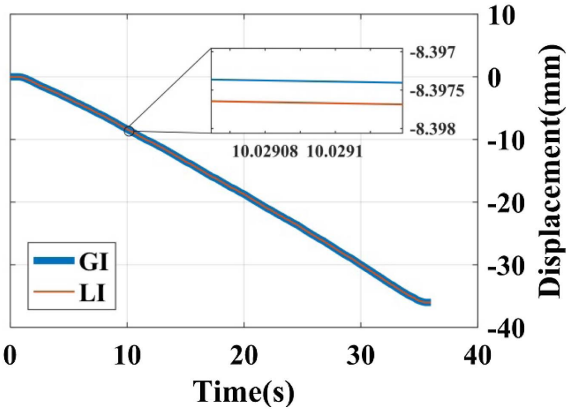


**Fig. 8.** Displacements measured using the LI and the GI. The red line represents the displacement measured by the GI with two incident beams in the crossed state. The blue line represents the displacement measured by the LI.

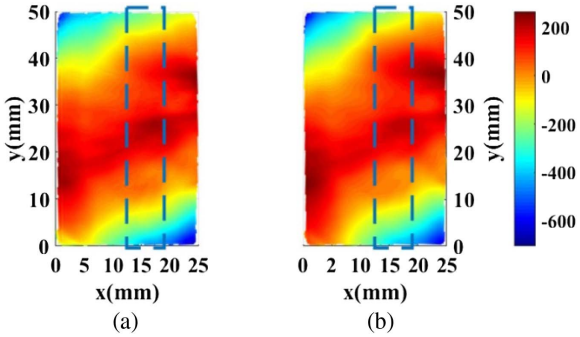


**Fig. 9.** Diffraction wavefronts of (a) the first order and (b) the −1st order of the grating.

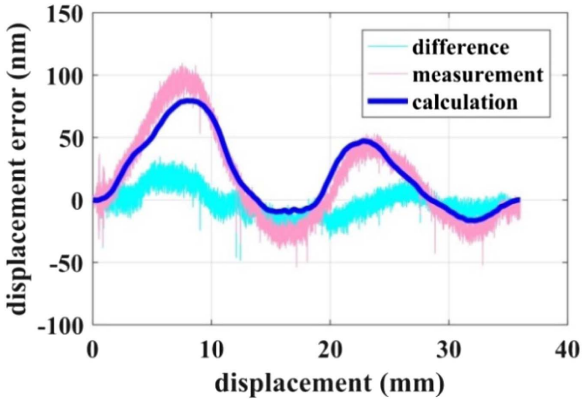


**Fig. 10.** Displacement errors of the grating with beam separated incidence. The dark blue line is the displacement error that was calculated using the diffraction wavefronts of the ±1st orders. The pink line shows the displacement error obtained from the displacement measurements when the GI is compared with the LI.

We extract the parts that are covered by the two beam spots from the diffraction wavefronts over the entire grating, which are the parts indicated by the dotted lines in the figures. From Fig. 9, we see that the peak-to-valley values of the ±1st-order diffraction wavefront curves are 535.21 and 485.45 nm. Because the Zygo interferometer and the GI operate at the same wavelength, the displacement error can be calculated directly from the diffraction wavefronts.

Figure 10 shows the measured and calculated displacement error results in the case of separated incidence. The calculated displacement error is closely matched with the measured value. The difference between them fluctuates around zero, and the $3\sigma$ value is 35.13 nm. The difference between the two results could be caused by misalignment of the two mirrors in the GI, the straightness of the linear stage, and changes in the surrounding environment. In addition, the beam spots have specific sizes, and the grating surface roughness and line density may vary within these beam spots. The phases caused by the grating surface error and the line error should be the average effects within the range of the beam spots. Therefore, the displacement error will differ from that in the ideal case, but the impact of this difference is small. This is because the beam spots

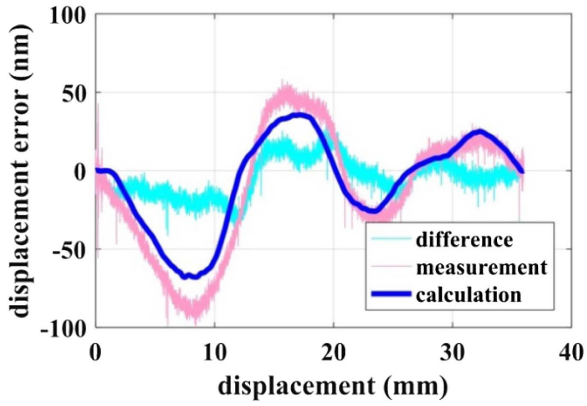


**Fig. 11.** Displacement errors of the grating with beam crossed incidence. The dark blue line is the displacement error that was calculated using the diffraction wavefronts of the ±1st orders. The pink line shows the displacement error obtained from the displacement measurements when the GI is compared with the LI.

are small, and the grating surface error and the line error do not mutate too greatly.

Figure 11 shows the measured and calculated results for the grating displacement error in the case of crossed incidence. The displacement error is different because of the different incident states of the two beams. However, the calculated displacement error results again coincide with the measured results. The difference between the two results is 37.80 nm ($3\sigma$). The possible causes of this difference are the same as those in the previous case.

## 4. DISCUSSION

In this section, we will discuss the effects of the accuracy of the precision linear stage and the misalignment of the two mirrors in the GI on the displacement error.

During the experiment, the grating is fixed on a precise linear stage. The pitch, roll, and yaw of this precise linear stage will change the grating angle directly. The pitch and roll of the grating hardly change the optical path of the two interference beams. However, the yaw of the grating changes the optical path of the two beams, which then has a greater effect on the displacement. Figure 12 shows a schematic diagram of the grating with a yaw angle of $\alpha$. The grating lies parallel to the $x$ axis, and the beams are ideally incident on points A and B of the grating at the Littrow angle $\theta$. When the grating

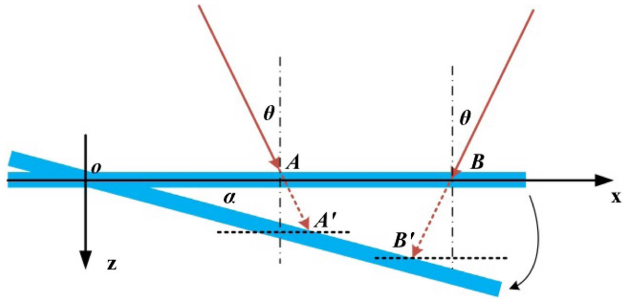


**Fig. 12.** Schematic diagram of grating with yaw angle $\alpha$.

rotates around point O at an angle $\alpha$, the points of incidence of the two beams become points $A'$ and $B'$. Because $\alpha$ is small, we can neglect the optical path changes caused by the changes in the diffraction angles. It can be seen from Fig. 12 that the optical paths of the two beams are increased by $2l_{AA'}$ and $2l_{BB'}$. According to their geometric relationship, the lengths of the line segments $AA'$ and $BB'$ are given by

$$l_{AA'} = \frac{l_{\mathrm{OA}} \sin \alpha}{\cos(\theta + \alpha)}, \tag{11}$$

$$l_{BB'} = \frac{(l_{\mathrm{OA}} + l_{AB}) \sin \alpha}{\cos(\theta - \alpha)}, \tag{12}$$

where $l_{\mathrm{OA}}$ is the length of line segment OA, and $l_{AB}$ is the length of line segment AB. The displacement measurement error is given by

$$x_{\mathrm{error}} = \frac{d}{4\pi m}\left[\frac{2\pi}{\lambda} 2(l_{BB'} - l_{AA'})\right] \approx \frac{l_{AB}\alpha}{\sin 2\theta}. \tag{13}$$

Equation (13) indicates that the displacement measurement error caused by the yaw of the grating is related to the distance between the two beam spots, the yaw angle, and the Littrow angle. If the yaw angle is 2 μrad and the distance between the two beam spots is 8 mm, then the error is approximately 17 nm. This error will affect the displacement measurement accuracy significantly.

Ideally, the incident and diffraction beams coincide, and the angle of incidence is equal to the diffraction angle. These angles are then all equal to $\theta$. When the mirrors in the GI are misaligned, the angles of incidence and diffraction will change. By differentiating both sides of the grating equation $d(\sin \theta_i + \sin \theta_q) = m\lambda$, we obtain

$$\cos \theta_i d\theta_i + \cos \theta_q d\theta_q = 0, \tag{14}$$

where $\theta_i$ is the angle of incidence, and $\theta_q$ is the diffraction angle.

In the Littrow configuration, $\theta_i = \theta_q$. Therefore, Eq. (14) can be written as

$$d\theta_i = -d\theta_q. \tag{15}$$

The absolute value of the variation of the diffraction angle is the same as that of the angle of incidence. When the angle of incidence becomes $\theta - \sigma$, the diffraction angle becomes $\theta + \sigma$, as shown in Fig. 13.

Without consideration of the errors, the displacement measurement principle of the GI is given by

$$I \sim \cos\left(4\pi m \frac{x}{d}\right), \tag{16}$$

where $m$ is the diffraction order, $x$ is the displacement, and $d$ is the period of the grating. It can be seen from Eq. (16) that the angle does not affect the displacement measurement of the GI. However, Eq. (6) indicates that the angle will affect the diffraction wavefront when there is a surface error in the grating, which will then affect the accuracy of the displacement measurement error caused by the grating surface error. When the mirrors are misaligned, Eq. (3) becomes

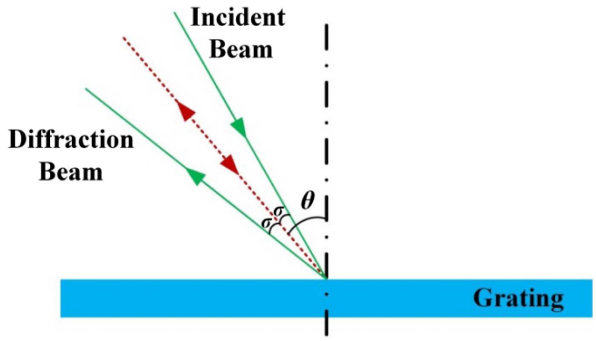


**Fig. 13.** Schematic diagram of the changes in the angle of incidence and the diffraction angle.

$$\begin{aligned}\delta_h' &= h(x_p, z_{pi})[\cos(\theta_m - \sigma) + \cos(\theta_m + \sigma)] \\ &= 2h(x_p, z_{pi}) \cos \theta_m \cos \sigma = \delta_h \cos \sigma.\end{aligned} \tag{17}$$

Equation (17) shows that when there is an error $\sigma$ in the angle of incidence, there will be a cosine error ($\cos \sigma$) in the optical path difference that is caused by the surface error. Equation (6) then becomes

$$\mathbf{\Delta}'(\pm m) = \mathbf{H} \cos \theta_m \cos \sigma_{\pm m} \pm \mathbf{W}\frac{m\lambda}{d}, \tag{18}$$

where $\sigma_{\pm m}$ are the diffraction angle errors of the $\pm m$th orders. Equation (10) then becomes

$$\mathbf{l_{ge}} = \frac{1}{2 \tan \theta_n}(\mathbf{H_1} \cos \sigma_{+n} - \mathbf{H_2} \cos \sigma_{-n}) + \frac{1}{2}(\mathbf{W}_1 + \mathbf{W}_2). \tag{19}$$

Therefore, misalignment of the mirrors in the GI causes the cosine errors to exist in the displacement errors caused by the grating surface errors. Because of the limitations of the beam spot sizes, the receivers and the other optical elements, the angles $\sigma_{\pm n}$ are very small. Therefore, the cosine errors will be small and can be neglected.

## 5. CONCLUSION

In conclusion, the surface error and the line error of the grating will both affect the displacement measurement accuracy of a GI with a Littrow configuration. The method proposed here can calculate the displacement error that is caused by the surface error and the line error quickly and accurately. Experiments showed that the differences between the calculated and measured displacement errors were less than 40 nm, which verified the correctness of the proposed method. Using this method, we can obtain the error curve, which is helpful in compensating for the errors and reducing the grating precision requirements. Scientific developments mean that the measurement range and precision requirements of GIs are constantly increasing. Large-sized gratings will be used in GIs, and the effects of surface errors and line errors in these gratings on the displacement cannot be ignored. Therefore, the proposed method will play an important role in error compensation. However, improvement of the calculation precision and determination of a convenient method to compensate for the system error using the

displacement error curve that can be calculated using the proposed method will require further study.

**Funding.** Jilin Province Science & Technology Development Program Project in China (20180201035GX); Jilin Province Special Funds for High-tech Industrialization in cooperation with the Chinese Academy of Sciences (CAS) (2018SYHZ0014); National Natural Science Foundation of China (NSFC) (61227901); Science and Technology Project of Changchun (17SS025).

**Acknowledgment.** We thank Dr. Hongzhu Yu, Shuo Li, and Jun Qiu for their useful suggestions and assistance in this work.

## REFERENCES

1. M. Malinauskas, A. Zukauskas, S. Hasegawa, Y. Hayasaki, V. Mizeikis, R. Buividas, and S. Juodkazis, "Ultrafast laser processing of materials: from science to industry," Light Sci. Appl. **5**, e16133 (2016).
2. A. C. Urness, M. C. Cole, K. K. Kamysiak, E. R. Moore, and R. R. McLeod, "Liquid deposition photolithography for submicrometer resolution three-dimensional index structuring with large throughput," Light Sci. Appl. **2**, e56 (2013).
3. K. Sugioka and Y. Cheng, "Ultrafast lasers—reliable tools for advanced materials processing," Light Sci. Appl. **3**, e149 (2014).
4. S. M. Jing, X. Y. Zhang, J. F. Liang, C. Chen, Z. M. Zheng, and Y. S. Yu, "Ultrashort fiber Bragg grating written by femtosecond laser and its sensing characteristics," Chin. Opt. **10**, 449–454 (2017).
5. B. G. Chen, M. Ming, and T. Y. Lv, "Precise measurement of curvature radius for spherical mirror with large aperture," Chin. Opt **7**, 163–168 (2014).
6. Q. Lv, W. H. Li, Bayanheshig, Y. Bai, Z. W. Liu, and W. Wang, "Interferometric precision displacement measurement system based on diffraction grating," Chin. Opt **10**, 39–50 (2017).
7. X. Xing, D. Chang, P. C. Hu, and J. B. Tan, "Spatially separated heterodyne grating interferometer for eliminating periodic nonlinear errors," Opt. Express **25**, 31384–31393 (2017).
8. Z. Tao, J. W. Cui, and J. B. Tan, "Simultaneous multi-channel absolute position alignment by multi-order grating interferometry," Opt. Express **24**, 802–816 (2016).
9. C. C. Hsu, H. Chen, C. W. Chiang, and Y. W. Chang, "Dual displacement resolution encoder by integrating single holographic grating sensor and heterodyne interferometry," Opt. Express **25**, 30189–30202 (2017).
10. X. H. Li, W. Gao, H. Muto, Y. Shimizu, S. Ito, and S. Y. Dian, "A six-degree-of-freedom surface encoder for precision positioning of a planar motion stage," Precis. Eng. **37**, 771–781 (2013).
11. E. Z. Zhang, B. Y. Chen, H. Zheng, L. Yan, and X. Y. Teng, "Laser heterodyne interferometer with rotational error compensation for precision displacement measurement," Opt. Express **26**, 90–98 (2018).
12. Y. T. Lou, L. P. Yan, B. Y. Chen, and S. H. Zhang, "Laser homodyne straightness interferometer with simultaneous measurement of six degrees of freedom motion errors for precision linear stage metrology," Opt. Express **25**, 6805–6821 (2017).
13. C. F. Kao, S. H. Lu, H. M. Shen, and K. C. Fan, "Diffractive laser encoder with a grating in Littrow configuration," J. Appl. Phys. **47**, 1833–1837 (2008).
14. C. C. Wu, C. C. Hsu, J. Y. Lee, and Y. Z. Chen, "Heterodyne common path grating interferometer with Littrow configuration," Opt. Express **21**, 13322–13332 (2013).
15. Y. C. Lu, C. L. Wei, W. Jia, S. B. Li, J. J. Yu, M. K. Li, C. C. Xiang, X. S. Xiang, J. Wang, J. Y. Ma, and C. H. Zhou, "Two-degree-freedom displacement measurement based on a short period grating in symmetric Littrow configuration," Opt. Commun. **380**, 382–386 (2016).
16. L. Šiaudinytė, G. Molnar, R. Köning, and J. Flügge, "Multi-dimensional grating interferometer based on fibre-fed measurement heads arranged in Littrow configuration," Meas. Sci. Technol. **29**, 054007 (2018).
17. Q. Lv, Z. W. Liu, W. Wang, X. T. Li, S. Li, Y. Song, H. Z. Yu, Bayanheshig, and W. H. Li, "Simple and compact grating-based heterodyne interferometer with the Littrow configuration for high-accuracy and long-range measurement of two-dimensional displacement," Appl. Opt. **57**, 9455–9463 (2018).
18. M. Sawabe, F. Maeda, Y. Yamaryo, T. Simomura, Y. Saruki, T. Kubo, H. Sakai, and S. Aoyagi, "A new vacuum interferometric comparator for calibrating the fine linear encoders and scales," Precis. Eng. **28**, 320–328 (2004).
19. R. J. Hocken, D. L. Trumper, and C. Wang, "Dynamics and control of the UNCC/MIT sub-atomic measuring machine," CIRP Ann. **50**, 373–376 (2001).
20. A. Wechkenmann and J. Hoffmann, "Long range 3 D scanning tunnelling microscopy," CIRP Ann. **56**, 525–528 (2007).
21. S. Yokozeki and S. Sawa, "Interferometric testing of gratings using Moiré method," Jpn. J. Appl. Phys. **14**, 465–470 (1975).
22. Z. Jaroszewicz, "Interferometric testing of the spacing error of a plane diffraction grating," Opt. Commun. **60**, 345–349 (1986).
23. X. T. Li, Bayanheshig, X. D. Qi, H. L. Yu, and Y. G. Tang, "Two-dimensional fast Fourier transform method of analyzing the influence of plane grating's line error and surface error on grating's spectral performance," Acta Opt. Sin. **32**, 1105001 (2012).
24. W. Gao and A. Kimura, "A fast evaluation method for pitch deviation and out-of-flatness of a planar scale grating," CIRP Ann. **59**, 505–508 (2010).